The collimation angle shift of desorbing product N_2 in a steady-state N_2O+CO reaction on Rh(110)

Tatsuo Matsushima[a] and Osamu Nakagoe
Catalysis Research Center, Hokkaido University, Sapporo 001-0021, Japan

Kosuke Shobatake
Toyota Physical and Chemical Research Institute, Nagakute, Aichi 480-1192, Japan

Anton Kokalj
Jožef Stefan Institute, 1000 Ljubljana, Slovenia

(Received 14 April 2006; accepted 15 August 2006; published online 3 October 2006)

The angular distribution of desorbing product N_2 was studied in N_2O decompositions on Rh(110) in the temperature range of 60–700 K. The N_2 desorption collimates along 62°–68° off normal toward either the [001] or [00$\bar{1}$] direction in a transient N_2O decomposition below ca. 470 K or in the steady-state N_2O+CO reaction above 540 K. In the steady-state reaction at the temperature from ca. 470 to 540 K, however, the collimation angle shifts from 62° to 45° with decreasing surface temperature. This angle shift is ascribed to the steric hindrance by coadsorbed CO because the N_2 collimation in transient N_2O decomposition at around 65° is recovered in the range of 380–500 K by an abrupt CO pressure drop followed by the decrease in CO coverage. N_2O is oriented along the [001] direction before dissociation. A scattering model of the nascent N_2 by adsorbed CO is proposed, yielding smaller collimation angles. © *2006 American Institute of Physics*.
[DOI: 10.1063/1.2352744]

I. INTRODUCTION

Nitrous oxide (N_2O) decomposition on rhodium surfaces has attracted much attention in the catalytic removal of nitrogen oxides in automobile exhaust gases because this metal is the best catalyst for the deNOx process and N_2O is one of the undesired by-products.[1] Its decomposition largely shares the N_2 emission in the NO reduction.[2] Furthermore, it has provided the first example of collimated fragment desorption in thermal decompositions on metal surfaces.[3,4] We deliver the first report of the collimation angle of desorbing N_2 on Rh(110) in a wide surface-temperature range (60–700 K). A significant shift of the collimation angle observed at 450–540 K is proposed to be due to a hindrance by coadsorbed CO.

Sharply collimated fragment desorption has frequently been reported in electron-stimulated desorption ion angular distribution (ESDIAD), in which the flux of desorbing ions or neutral species is analyzed in an angle-resolved (AR) form when the surface is exposed to electron or photon beams.[5,6] In this method, the desorbing species frequently have high translational energies, and the desorption event can be induced in a very short interval.[7,8] Thus, the AR signal can be easily separated in simple time-resolved (TR) measurements from that of the species scattered in the reaction chamber and penetrating the analyzer. In thermal reactions, however, the translational energy of products is much less and the TR type cannot extract the AR signal because of the prolonged desorption event.[9] AR-product measurements for thermal desorption must be performed in an apparatus with *at least two slits and an extremely large pumping rate* either in the reaction chamber or in the collimator between the two chambers.[10]

Following this criterion, collimated product desorption in thermal reactions on metal surfaces has been limited to some kinds of associative desorption, such as $CO(a)+O(a) \rightarrow CO_2(g)$, $H(a)+H(a) \rightarrow H_2(g)$, and $N(a)+N(a) \rightarrow N_2(g)$.[9] In the *thermal decomposition of adsorbed molecules*, the product fragment is assumed to be thermalized to the surface temperature before desorption.[11] Therefore, the above N_2 emission from N_2O is exceptional because it is directly emitted in a thermal dissociation event (without an associative process). A sharply collimated fragment emission was once reported in a hydrazine decomposition on Ir(111) in 1980.[12] However, the reliability of the AR signal is not clear, since the measurements were performed in an apparatus with a single slit.

In the above associative processes, the product desorption sharply collimates along the local normal of the product-formation site.[9] On the other hand, in the N_2O decomposition on Pd(110), Ir(110), and Rh(110), the N_2 desorption is split into a two-directional way in the plane along the [001] direction.[4] The emitted N_2 on Pd(110) has a hyperthermal energy and holds structural information on the parent molecule because adsorbed N_2O is oriented along the [001] direction and the N_2 emission is highly concentrated in the plane along this direction.[3,13] In particular, the fragment N_2 on Rh(110) is emitted closely parallel to the surface plane. Thus, it may be scattered by coadsorbed species on its trajectory or the dissociation itself may be hindered, yielding a collimation angle that depends on the reaction condition.

[a]Fax: 81-11-706-9120; Electronic mail: tatmatsu@cat.hokudai.ac.jp

This effect can be examined by comparing the N_2 collimation angles in the steady-state and the transient N_2O reduction by CO because the coverage of adsorbed CO can be reduced to a lower level in the transient N_2O reduction in the temperature range of 400–500 K.[14] On the other hand, the surface is highly covered by CO in the steady-state N_2O +CO reaction under reducing conditions in the same temperature range.[15]

The N_2O decomposition itself is sensitive to the surface structures. The desorption of adsorbed N_2O is completed below 200 K without dissociation on Pt(111), Ir(111), Ni(111), Ag(111), and Rh(111).[16–20] On the other hand, on open surfaces such as Rh(110), Pd(110), Cu(110), Ni(110), Ni(100), and stepped Ni(557), it dissociates below 200 K.[20–22] Fortunately, the N_2O decomposition continues as long as the deposited oxygen is removed by reducing reagents such as CO and H_2 and thus the surface-nitrogen removal is not rate determining.[14] Even in such a case, the angular and velocity distributions provide information on the product desorption process because they do not involve the reaction rate and are controlled only by the desorption process.

II. EXPERIMENT

Two ultrahigh vacuum (UHV) apparatuses composed of a reaction chamber, a chopper (or collimator) house, and an analyzer were used. Both have an ion gun and a mass spectrometer (MS) for angle-integrated (AI) measurements in the first chamber and another MS in the analyzer. One was used for the investigation of N_2O decomposition both in the steady-state N_2O reduction at surface temperatures (T_S) above 450 K and after a rapid CO pressure drop (PD) in the range of 370–500 K. This apparatus had low-energy electron diffraction (LEED) and x-ray photoelectron spectroscopy (XPS) optics and a cross-correlation chopper blade for time-of-flight (TOF) analyses.[9] This chopper house was evacuated by a 25-K-cooled copper plate yielding a pumping rate of about 7 m^3/s as well as a tandem-turbomolecular pumping system. The distance from the ionizer to the chopper blade is 377 mm, and the time resolution was set at 20 μs. The other apparatus used for N_2O pressure jump (PJ) experiments at T_S=60–400 K has a cryoplate in the reaction chamber yielding a pumping rate of about 9 m^3/s and allows cooling a sample below 50 K.[23] A Rh crystal with (110) surfaces was rotated to change the desorption angle (θ: polar angle) in the plane along the [001] direction.[2]

The crystal was cleaned by repeated cycles of Ar^+ ion bombardments, oxygen treatments at 850 K, and annealing to 1200 K until a sharp (1×1) LEED structure or the reproducible oxygen temperature-programmed desorption (TPD) curve was observed. The cleanliness of the surface was verified by the absence of CO and CO_2 desorption in TPD after oxygen exposure.[24] Before each experiment, the surface was annealed at 1200 K for 5 min to remove the surface oxides.[23]

Without further purification, $^{15}N_2O$ (the isotope purity: 99%) was introduced through a gas doser while ^{13}CO (the isotope purity: 99%) was backfilled. The product signals of $^{15}N_2$ and $^{13}CO_2$ were mostly monitored in the AR form. Hereafter, ^{15}N and ^{13}C are simply denoted as N and C in the text. The AR signal in the steady-state reaction was obtained by the MS in the analyzer as the difference between the signal at the desired angle and that when the crystal was away from the line-of-sight position.

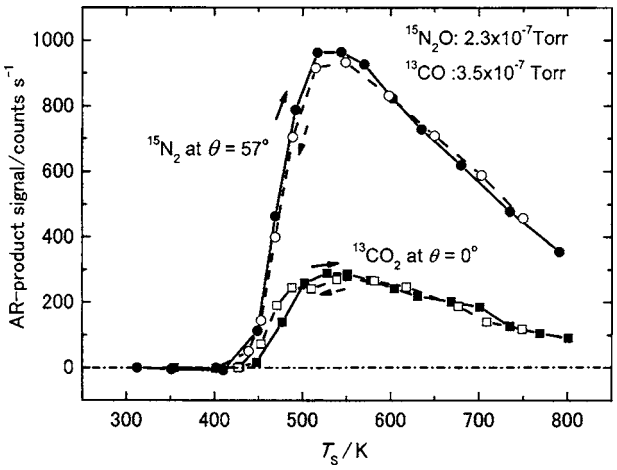

FIG. 1. Temperature dependence of AR signals of $^{13}CO_2$ at the surface normal and of $^{15}N_2$ at θ=57° in the plane along the [001] direction in the steady-state $^{15}N_2O+^{13}CO$ reaction on Rh(110). $P_{N_2O}=2.3\times10^{-7}$ Torr and $P_{CO}=3.5\times10^{-7}$ Torr. The signals observed while the surface temperature was increased are designated by closed symbols and those in the downward direction by open symbols.

Under this construction, the flux of incident N_2O towards the unit surface area decreases when the angle is shifted from the normal direction. This effect was corrected as previously described in detail.[25] However, the N_2O pressure in the figures shows the value when the gas was dosed from the normal direction. The fragmentation of N_2O into N_2 in both mass spectrometers was separately estimated by introducing N_2O and corrected. In this report, all the partial pressures were corrected by the sensitivities of a Bayart-Alpert (BA) gauge. This calibration against the BA reading was performed by comparing the CO_2 yield when N_2O was supplied from the doser with that when N_2O was backfilled.

III. RESULTS

A. General features of the steady-state N_2O reduction

The AI signal of the product N_2 involves large experimental uncertainty because of the large background N_2 formation. On the other hand, the AR N_2 signal is reliable on account of the sharply collimated desorption. The AR N_2 signal at θ=57° [the maximum flux position (collimation angle) at 500 K] is shown versus T_S under a reducing condition at $P_{N_2O}=2.3\times10^{-7}$ Torr and $P_{CO}=3.5\times10^{-7}$ Torr (Fig. 1). As described in detail below, depending on the reaction conditions, the N_2 desorption collimates sharply in the range of 43°–66° off the surface normal in the plane along the [001] direction.

The N_2 signal becomes noticeable above 410 K, increases quickly to the maximum, and then decreases slowly at higher temperatures. With decreasing CO pressure, the starting temperature shifts to lower values; however, a significant hysteresis is found versus surface-temperature variation when $P_{CO}<P_{N_2O}$. The AR CO_2 signal in the normal

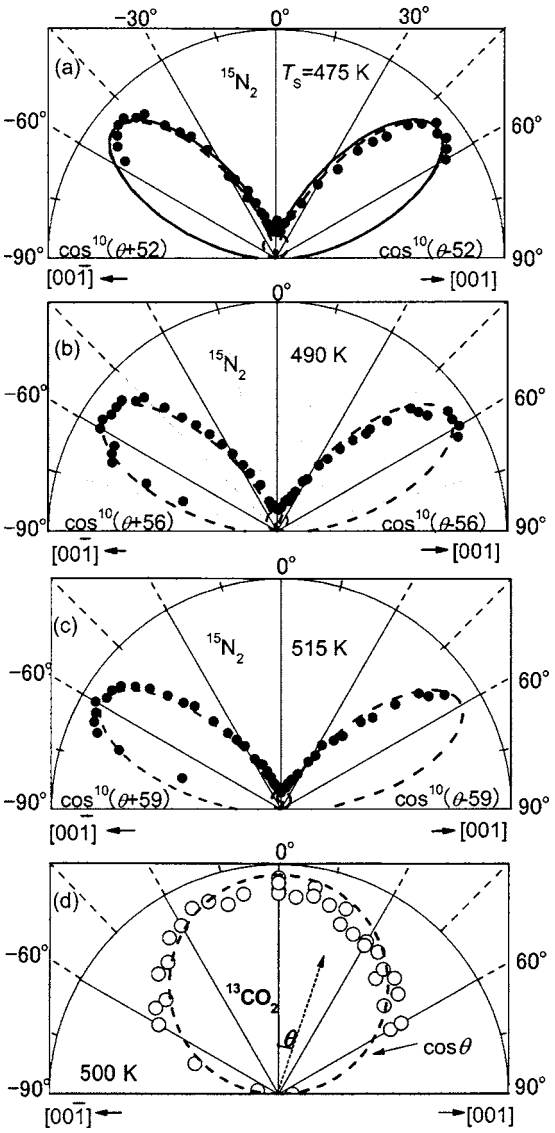

FIG. 2. Angular distributions of desorbing $^{15}N_2$ and $^{13}CO_2$ in the plane along the [001] direction in the steady-state $^{15}N_2O+^{13}CO$ reaction. T_S (K) =(a) 475, (b) 490, and (c) 515 for $^{15}N_2$, and (d) 500 for $^{13}CO_2$. $P_{N_2O}=2.3\times10^{-7}$ Torr and $P_{CO}=3.5\times10^{-7}$ Torr. The broken curves are based on the inserted power functions of the cosine of the desorption angle shift. The solid line shows the sum of the components. Notice that the collimation angle of N_2 shifts with increasing surface temperature.

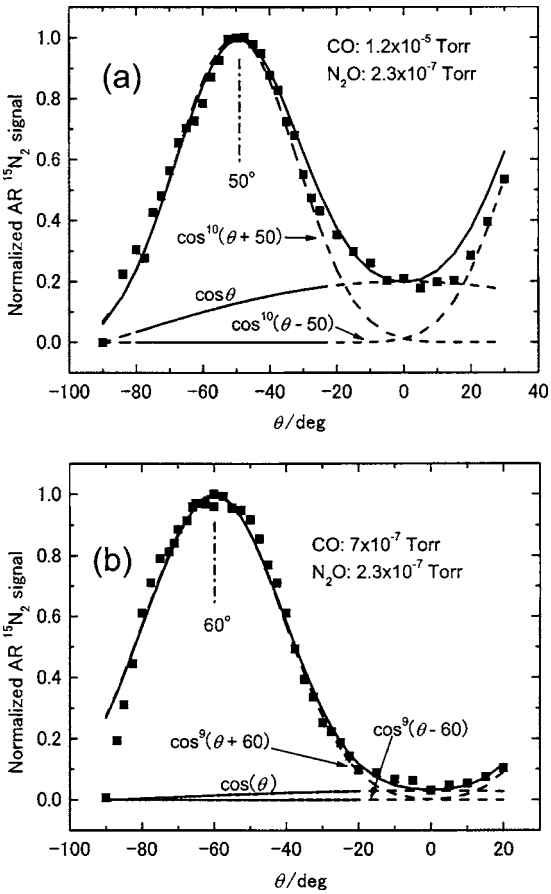

FIG. 3. CO pressure effect on the collimation angle. The angular distributions of desorbing $^{15}N_2$ in the plane along the [001] direction in the steady-state N_2O+CO reaction at T_S=520 K. $P_{N_2O}=2.3\times10^{-7}$ Torr and $P_{CO}(\times10^{-7}$ Torr)=(a) 120 (high CO) and (b) 7 (low CO). The broken curve is based on the inserted power functions of the cosine of the desorption angle shift from the collimation angle. The solid line shows their sum. Notice that the collimation angle shifts with increasing CO pressure.

direction shows a temperature dependence similar to that of N_2. The difference in their signals is due to different angular and velocity distributions.

The surface under reducing conditions shows a (1×1) LEED pattern as expected.[26,27] Sharp changes in the LEED spot intensity were found at approximately the kinetic transition (KT) around $P_{CO}/P_{N_2O}=1$. The well-known $(2\times2)p2mg$-O structure appeared at low P_{CO} and its LEED intensity was fairly constant below KT. With increasing P_{CO} value, the half-order spots disappeared at around KT.

B. Angular distributions in the steady-state reduction

The angular distribution of desorbing N_2 collimates far from the surface normal in the plane along the [001] direction (Fig. 2). The distribution depends on both the CO pressure and the surface temperature. The distribution was approximated by the sum of two symmetric power functions of the cosine of the angle shift from the collimation position and the cosine distribution component as shown in Figs. 2(a) and 3. With decreasing surface temperature in the range of 540–446 K, the collimation angle shifts from 65° at 520 K to 45° at 446 K at 3.5×10^{-7} Torr of CO (Fig. 4). Above 540 K, the collimation angle somewhat decreases with increasing surface temperature to around 63°. The distribution itself becomes slightly sharper at temperatures below 520 K. It is difficult to examine the angular distribution in the steady-state N_2 formation below 440 K. At high CO pressures, the reaction rate decreases, and the cosine component is relatively enhanced, reaching about 20% of the signal in the normal direction [Fig. 3(a)]. This cosine component decreases at lower CO pressures and becomes negligible at 5×10^{-7} Torr at 520 K [Fig. 3(b)]. The angular distribution of the inclined desorption is broader than that in the N_2O reduction on Pd(110) showing a $\cos^n(\theta-45)$ form with n =14–28.[28] The CO_2 desorption follows a simple cosine distribution [Fig. 2(d)], consistent with the results in the CO oxidation under reducing conditions, i.e., in the region inhibited by CO.[29]

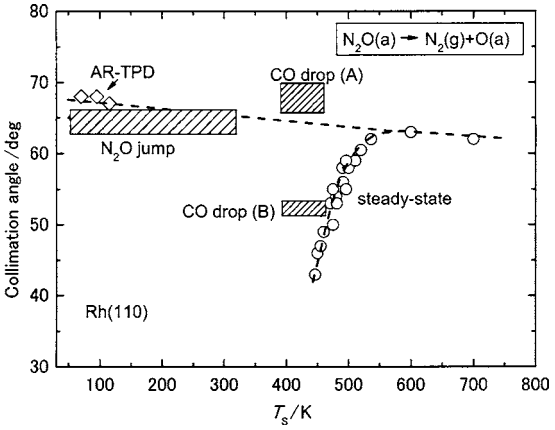

FIG. 4. Temperature dependence of the collimation angle of desorbing $^{15}N_2$ formed in N_2O decomposition. Open circles: the steady-state N_2O+CO reaction at $P_{N_2O}=2.3\times10^{-7}$ Torr and $P_{CO}=3.5\times10^{-7}$ Torr. CO drop: collimation angle attained following the CO pressure drop induced by the CO flux termination from the steady reduction condition (A) at low CO(*a*) coverages and (B) at high CO(*a*) density (see the text). N_2O jump: N_2O dosed to a clean surface. AR-TPD: temperature-programed desorption of N_2O-covered Rh(110) (see Ref. 23).

C. Velocity distribution at 450–800 K

The velocity distribution curves of desorbing N_2 at the collimation angle at 550 and 460 K are shown in Fig. 5. The apparent translational temperature calculated as $T_{\langle E\rangle}=\langle E\rangle/2k$ is shown in angular brackets in the figure, where $\langle E\rangle$ is the average kinetic energy and k is the Boltzmann constant. The value at $T_S=550$ K is maximized to 3520 K around the collimation angle. It decreases slowly with increasing shift from the collimation position. The distribution includes a small amount of the component expected by the Maxwell distribution at the surface temperature which yields the cosine component. This is consistent with very small amounts of the cosine component observed in the angular distribution. The apparent translational temperature at the collimation angle decreases with decreasing surface temperature, especially below 540 K as shown in inset (c).

This decrease is due to the suppression of the faster part. In order to show this clearly, the velocity curves were deconvoluted as follows. The velocity curve itself is still wide even after the subtraction of the thermalized component, yielding about 1.24 in a wide T_S range for the speed ratio defined as $(\langle\nu^2\rangle/\langle\nu\rangle^2-1)^{1/2}/(32/9\pi-1)^{1/2}$, where ν is the velocity of the molecule, $\langle\nu\rangle$ is the mean velocity, and $\langle\nu^2\rangle$ is the mean square velocity. The speed ratio is usually below unity for a hyperthermal component at around the collimation position, suggesting two components.[11] Hence, the distribution curve was deconvoluted into two components, each of which has a modified Maxwellian distribution, $f(\nu)=\nu^3\exp\{-(\nu-\nu_0)^2/\alpha^2\}$, where ν_0 is the stream velocity and α is the width parameter. It should be noted that this fitting form has no physical background. Thus, we simply assumed a common width parameter for the deconvolution procedures.[25] The resultant deconvolutions are shown by broken curves. The faster component at $T_S=550$ K gives the apparent translational temperature of about 7700 K, and the slower one, about 2600 K. With decreasing surface temperature, the faster component is quickly suppressed, making the slower one predominant.

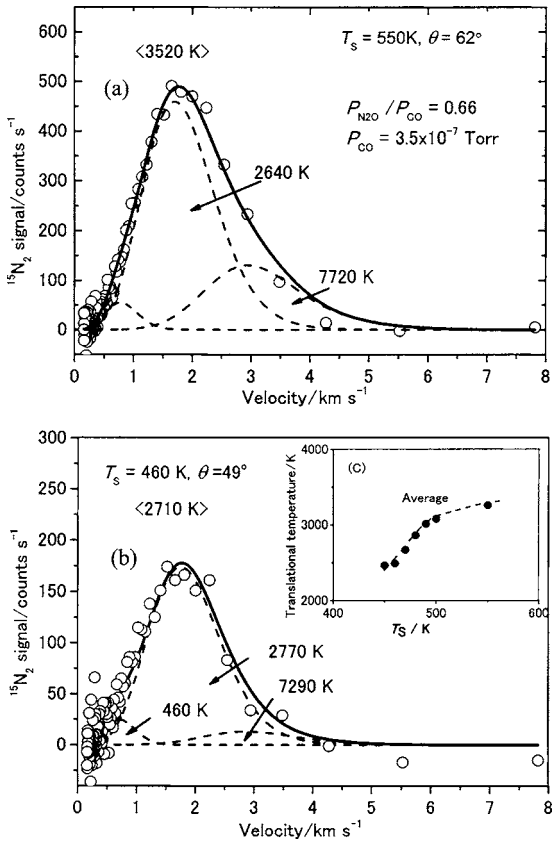

FIG. 5. Velocity distributions of desorbing $^{15}N_2$ in the steady-state $^{15}N_2O+^{12}CO$ reaction at the collimation angle. (a) $T_S=550$ K and 62° and (b) $T_S=460$ K and 49°. $P_{N_2O}=2.3\times10^{-7}$ Torr and $P_{CO}=3.5\times10^{-7}$ Torr. The average kinetic energy is given in angular brackets in temperature units. Typical deconvolutions into two fast components and a thermalized component are given by broken curves. The translational temperature for each component is also given. Open circles represent the observed signals. (c) Temperature dependence of the average kinetic energy.

The translational temperature on Rh(110) is found to be higher than the corresponding value in the N_2O reduction on Pd(110), although the angular distribution itself is broader than that on Pd(110). This is also consistent with the presence of two components in the inclined desorption on Rh(110).

D. Transient CO_2 and N_2 formations and CO coverage

The above-mentioned collimation angle shift is likely to be due to the effect of adsorbed CO rather than the surface temperature. The CO pressure effect suggests the scattering of the product or the blocking of N_2O dissociation by adsorbed CO. In order to confirm this effect, the N_2 distribution was examined at lower CO coverage. An enhanced N_2 emission can be transiently induced by a sudden termination of the CO supply from the steady-state reaction condition below about 500 K.[30] The N_2 emission takes place at CO coverage much lower than those under the steady-state reaction condition. Analyses of the time profiles of the AR N_2 signals manifest a backward shift of the collimation angle in the following manner.

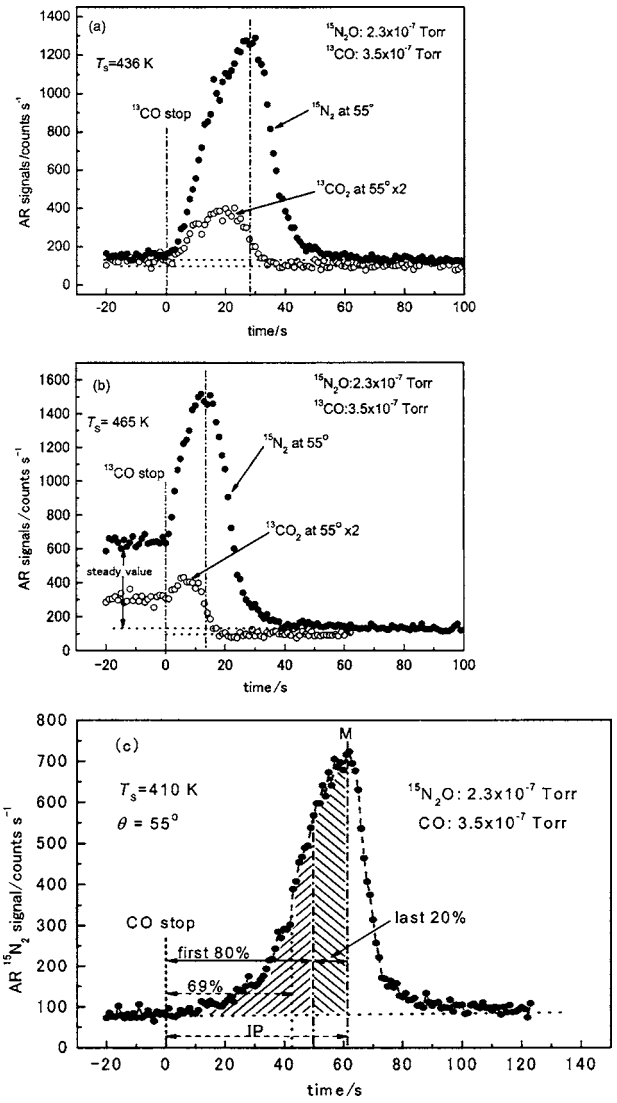

FIG. 6. Transient $^{15}N_2$ intensity vs time after the abrupt termination of ^{13}CO supply during the steady-state $^{15}N_2O$ reduction at $P_{N_2O}=2.3\times10^{-7}$ Torr and $P_{CO}=3.5\times10^{-7}$ Torr. (a) 436 K and (b) 465 K. The signal of $^{13}CO_2$ is twice magnified. (c) A N_2 transient curve at 410 K and its analysis. The percent (%) sign marks the relative time intervals.

After the steady-state reaction has been established, the CO supply is quickly stopped while the N_2O dosage is kept constant and the AR signals of N_2 and CO_2 are monitored at $\theta=55°$ as a function of time. Both the CO_2 and N_2 signals exhibit respective maxima after respective durations depending on the surface temperature. Typical variations of both signals are shown in Fig. 6. The large intensity difference in the signals between CO_2 and N_2 is mostly due to the difference in their angular distributions. At T_S=436 K, the AR CO_2 signal increased to a maximum at 19 s after the CO valve closure and rapidly dropped to the background level. This CO_2 product comes from the reaction of CO adsorbed on the surface before cutting off the CO supply. The CO adsorption during the transient period was negligible because its pressure decreased to a negligible level within 2 s. Hence, the area under the CO_2 curve conserved the CO coverage during the steady-state reaction because the reaction CO(a) +O(a) is faster than the CO desorption.[31] This CO pressure drop can be used to estimate the CO coverage in the temperature range of 380–460 K. At higher temperatures, the CO coverage will be overestimated by the relatively large CO adsorption because of the short interval to the maximum signal. At 465 K, the CO_2 signal peaked at only 9 s. On the other hand, at 410 K, the CO_2 peak appeared at about 55 s. Below about 370 K, both the transient CO_2 and N_2 formations become weak and are extended over a long period.

The CO coverage was estimated from the CO_2 peak area induced by CO-PD in the presence of gaseous N_2O. The peak area of CO_2 is normalized to that in AI-TPD of CO at the same temperature, i.e., the conversion factor was estimated by a comparison of the CO TPD area with the peak area of CO_2 in the PD at 430 K. The CO coverage itself was estimated by AI-TPD in the presence of CO at $P_{CO}=3.5\times10^{-7}$ Torr and was normalized to the literature value of CO adsorption.[15] The resultant CO coverage in the steady-state N_2O reduction is equal to that in the absence of N_2O. This means that the adsorption and desorption of CO are in equilibrium in the course of the N_2O+CO reaction under reducing conditions in a way similar to that in the CO oxidation.[29] The CO coverage is around 1/2 ML at 460 K, where the reaction is largely suppressed and the collimation angle is 45°. The value is about 1/4 ML at 500 K, where the retardation begins and the collimation angle shift becomes noticeable.

The AR N_2 signal increases in a way similar to that of CO_2 after the CO supply is stopped. It should be noted that the peak position of the N_2 signal always appears close to the disappearance point of the CO_2 signal. This is consistent with the fast CO(a)+O(a) reaction, i.e., O(a) begins to be accumulated after CO(a) is mostly consumed. In other words, both CO(a) and O(a) prevent N_2O from dissociating, and the N_2 emission is then maximized at the point where CO(a) is mostly removed. The peak area of the N_2 signal cannot be used to measure the amount of adsorbed CO because of its strong temperature dependence. There are two cases for the N_2 emission, i.e., N_2O dissociation (i) without O(a) and (ii) with O(a) accumulation. These cases appear predominantly before and after the N_2 maximum, respectively, when the reaction of CO(a)+O(a) is fast. The area in (i) can be used as a monitor of the CO(a) amount, but that in (ii) decreases quickly with decreasing surface temperature. This remarkable temperature dependence has been confirmed on the clean surface as described in Sec. III F. On the present surface, in fact, the reaction of CO(a)+O(a) is not fast enough to clean off the surface below about 400 K and the CO_2 signal is still noticeable at the N_2 peak position, indicating the overlapping of the above two cases. In particular, below 360 K, the CO_2 peak appears after the N_2 maximum. Probably, separate domains of CO(a) and O(a) are formed,[32] and the removal of CO(a) is then not completed at the N_2 peak position.

E. Angular distribution in transient N_2O decomposition

The above-mentioned transient N_2 emission profile was analyzed in the angle-resolved way to get the angular distribution of desorbing N_2 at lower CO coverage. The variation of the N_2 peak area with desorption angles is shown in

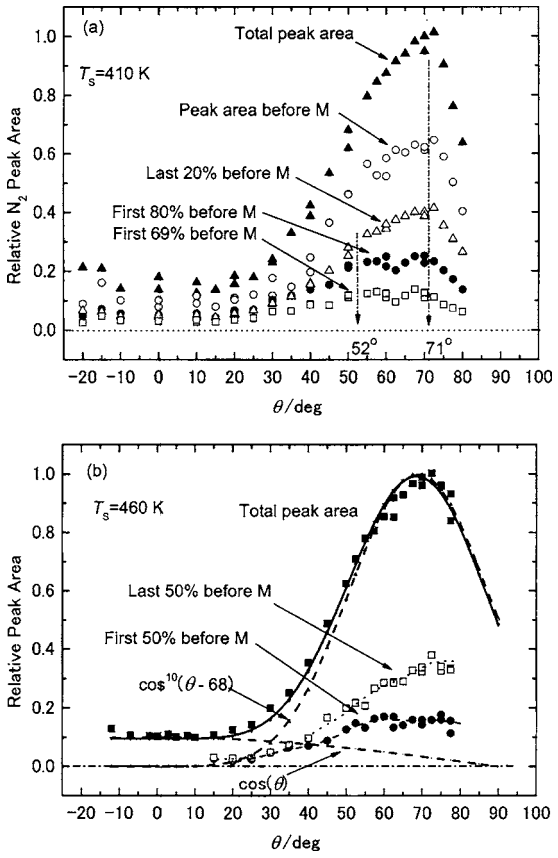

FIG. 7. Angular distributions of desorbing $^{15}N_2$ in the plane along the [001] direction in the transient N_2O decomposition induced from the steady-state reduction at $P_{N_2O}=2.3\times10^{-7}$ Torr and $P_{CO}=3.5\times10^{-7}$ Torr. (a) 410 K and (b) 460 K. The relative N_2 peak area until fixed periods is plotted vs desorption angle. The percent (%) sign marks the relative time intervals.

Fig. 7. The total N_2 signal area is maximized at 68°–70° at 410 K where the CO coverage reached 0.71 ML in the steady state and at 460 K where 0.47 ML of CO was reached under the steady-state reaction. However, the CO coverage largely decreased during the transient procedure. Especially, most of the N_2 is emitted after half of the CO is removed (Fig. 6), i.e., the collimation angle must shift in the course of the transient reaction if the shift is due to the CO effect. The collimation angle of 70° may be assigned to the N_2O decomposition at low CO coverage. In earlier parts of the transient reaction, the collimation angle is expected to shift to smaller values. This point was examined in the following way as shown in Fig. 6(c). At 410 K, the peak areas from the PD starting from the points of 69% and 80% of the period to the N_2 maximum [the induction period (IP)] are plotted versus the desorption angle [Fig. 7(a)]. In the former 69% period, the peak area shares about 13% of the total N_2 signal area. The N_2 emission in these earlier parts involves the desorption collimated at around 52° in addition to the component along 71° with a comparable intensity. The peak area for the first 80% period showed a similar angle dependence. On the other hand, the 71° component is predominant in the area of the last 20% period (before the N_2 maximum) in a similar way to that in the total peak area. These comparisons indicate that the emitted N_2 in an earlier PD part involves two desorption components collimated at around 50° and 70°. The latter component is relatively enhanced in later parts. This trend is also observed at 460 K [Fig. 7(b)], where the first 50% of the period to the N_2 maximum was selected. The total signal is approximated in a form of $\cos^{10}(\theta-68)+0.1\cos(\theta)$. However, this distribution has been already broadened by the contribution from the 50° component. This 50° component became clear in the presence of adsorbed CO. The 70° component was enhanced on the surface that is almost free from CO(a).

F. N_2 emission at low temperatures

N_2O itself is partly dissociated even at 60 K when it is dosed to clean Rh(110). The resultant N_2 emission profiles obtained at fixed temperatures were analyzed in the AR form. A typical trace of the AR N_2 signal at $\theta=70°$ and 64 K, as well as the AI signal, is shown in Fig. 8(a). The N_2 signal initially jumps and slowly decreases to the steady value which is due to the fragmentation of N_2O in the analyzer. The N_2O pressure was kept constant at 5.6×10^{-9} Torr. The amount of N_2 produced above the steady-state line at 140 K is plotted against the desorption angle in Fig. 8(b) because the incident N_2O flux decreases with increasing shift from the normal incidence since the angle between the incidence of N_2O exposure and the detection of desorbing N_2 was fixed at 45° in this apparatus.[23] The N_2 desorption is sharply collimated at around 65° off normal. The intensity was approximated as a $\cos^{10}(\theta-65)$ form except for a small contribution from the cosine component.

The maximum N_2 signal at the beginning of the exposure increased with increasing N_2O pressure, and the integrated amount above the fragment line remained invariant. This integrated amount increases with increasing fixed T_S as shown in Fig. 8(c). At around 200 K, it increases approximately four times that at 60 K. The amount above 300 K is likely to be underestimated because the signal itself becomes so small that the separation from the large background level is difficult.[20] In the figure, the results estimated from the AR signal at 65° and the AI one are shown. Both quantities show a similar temperature dependence, indicating no change in the angular distribution. In fact, the collimation angle remains at around 65° below 300 K (Fig. 4).

IV. DISCUSSION

A. Surface structures

Oxygen adsorption takes place dissociatively on Rh(110) at temperatures above 100 K and leads to various ordered phases.[26,27] At temperatures between 125 and 300 K, the $(2\times1)p2mg$ LEED pattern appears sharply at saturation. This has been recently analyzed by scanning tunneling microscopy (STM) to be due to the zigzag oxygen chains decorating adjacent $[1\bar{1}0]$ Rh rows on unreconstructed (1×1).[33] At lower converge, the (2×3) or (2×6) pattern appears. After annealing of oxygen-covered surfaces above 470 K, the surface shows a missing-row-type reconstruction. Several lattices are observed such as $(2\times2)p2mg$ and $c(2\times2n)$ with $n=3$, 4, and 5. STM work shows that the oxygen atoms form zigzag rows in the trough.[34–36] These oxygen atoms can be

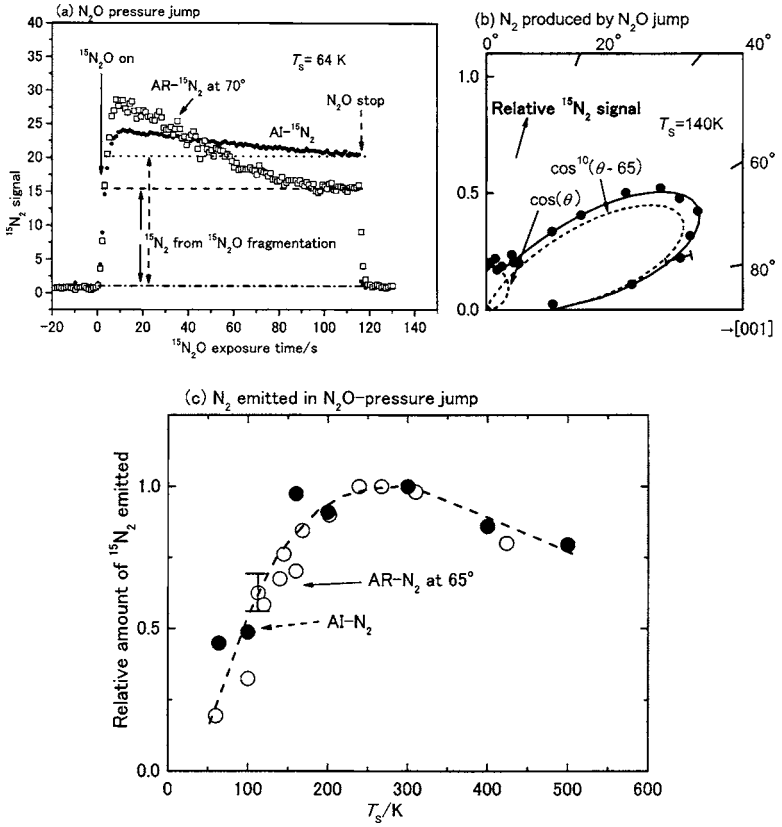

FIG. 8. $^{15}N_2$ emission in the $^{15}N_2O$ pressure jump on clean Rh(110). (a) The transient AR $^{15}N_2$ signal at 70° and AI signal when a clean Rh(110) at 64 K is exposed to a constant $^{15}N_2O$ flux equivalent to 5.6×10^{-9} Torr. (b) Angular distributions of desorbing $^{15}N_2$ formed in the $^{15}N_2O$ exposure at 140 K. The broken curves are drawn by the inserted power functions of the cosine of the desorption angle shift. (c) Variation of the relative amount of $^{15}N_2$ formed in the $^{15}N_2O$ exposure with surface temperatures. Open circles: the total formation estimated from AR $^{15}N_2$ signal at 65°. Closed circles: the amount estimated from the AI signal.

removed by hydrogen or CO so that the surface can remain in a (1×2) or $(1\times n)$ missing-row configuration.[37] This structure is metastable and can be converted back into a (1×1) form above about 480 K. Therefore, the (1×1) LEED pattern under reducing conditions is reasonable.

The adsorption energy and saturation coverage of CO are only slightly affected by the difference in structures between (1×1) and (1×2).[38] CO is slightly more strongly bound on the (1×1). At low coverage, a $p(2\times2)$ lattice appears in a diffuse form.[39] The repulsive interaction between CO becomes remarkable as the adlayer starts to form $c(2\times2)$ on the (1×1) or $c(2\times4)$ on the (1×2) surface. At present, it is not certain whether CO is located on atop or bridge sites. The $c(2\times2)$-CO on the (1×1) appears between 0.33 and 0.55 ML. At higher coverage, (4×2) and (5×2) symmetries appear. Finally, a sharp $(2\times1)p2mg$ pattern characteristic of the saturation coverage (1 ML) is observed. This dense structure disappears at 270–280 K (just below the desorption temperature), suggesting an order-disorder phase transition. Exposing the (1×2) surface to CO results in a $c(2\times4)$ at 0.40–0.63 ML and then $(2\times2)pg$ at 0.92 ML.

It is reasonable that adsorbed CO forms $p(2\times2)$ and then $c(2\times2)$ at higher coverage under the present reducing conditions. In the following, we will discuss N_2O dissociation on the Rh(110)(1×1) surface

B. Desorption components and adsorbed N_2O

The N_2 desorption resulting from N_2O decomposition on clean Rh(110) may be limited to only one component. In the previous AR-TPD work, we reported two collimated N_2 desorption components below 200 K.[23] One of them is collimated at 65°–70° off normal toward the [001] direction and the other is sharply collimated around 30°. The former was found on clean Rh(110) as well as on the surface with adsorbed oxygen. The latter was observed on a rhodium-oxidized surface. The oxide producing the 30° component was formed by annealing oxygen-covered Rh(110) above 500 K.[40] However, we did not find this component in the steady-state N_2O reduction in the temperature range of 450–800 K. The present experiments were limited under the reducing condition and therefore the oxide may have been reduced by CO. On the clean surface, four desorption peaks $(\beta_2-\beta_5)$, which appear at 70–140 K in AR-TPD of N_2O-covered Rh(110), commonly collimate along 65°–70° off normal.[23] Only this component appears in the steady-state reduction. The differences among $\beta_2-\beta_5$ N_2 peaks are due to surface modifications by deposited oxygen.[41]

The Rh(110) surface with oxygen is more or less reconstructed into the (1×2) missing-row structure above 300 K. The resultant surface is stabilized with O–Rh–O–Rh zigzag chains extending along the $[1\bar{1}0]$ direction.[36] This oxygen prevents N_2O from dissociating because the local oxygen coverage is 0.5 ML.[42] The surface structure under reducing conditions is (1×1), which is very active toward N_2O dissociation. With the surface temperature decreasing below 540 K, the N_2 distribution on Rh(110) narrows from a $\cos^9(\theta\pm62)$ form at 550 K to a $\cos^{13}(\theta\pm46)$ form at 450 K. This distribution is not as sharp as would be expected from the high translational temperature of approximately 3500 K. This is also in contrast to previous results, i.e., the product CO_2 in the *active region* of the CO oxidation on Rh(110)

shows a $\cos^{10}(\theta \pm 24)$ form and a translational temperature of approximately 1500 K,[29] and the product N_2 in the N_2O reduction on Pd(110) yields a $\cos^{18-28}(\theta \pm 45)$ form with a translational temperature of approximately 3000 K.[30] Roughly speaking, the sharper the angular distribution is, the higher the translational temperature is expected to be.[9,12] The broad N_2 distribution with a high translational temperature on clean Rh(110) suggests the presence of two or more components with sharper distributions.

For highly inclined N_2 desorption, the decomposition of N_2O oriented in the [001] direction was first proposed on Pd(110)(1×1) with N_2 collimated at 43°–50° into the [001] direction.[3] Within this mechanism, $N_2O(a)$ is initially lying and oriented in the [001] direction. Recent near-edge x-ray absorption fine-structure[43] (NEXAFS) and STM (Ref. 13) studies provided evidence for N_2O oriented along the [001] direction as well as N_2O standing upright with the terminal nitrogen interacting with metal atoms on Pd(110). However, this structure has not been experimentally confirmed on Rh(110). The lying configuration on both Pd(110)(1×1) and Rh(110)(1×1) has been predicted by a density-functional theory (DFT) calculation.[44,45] Thus, we assign the [001]-oriented N_2O as the precursor to dissociation.

C. CO(*a*) effect

It is interesting that both the angular distribution and the collimation angle of desorbing N_2 in the N_2O decomposition are insensitive to the surface temperature. The enhanced thermal motions at high temperatures do not affect the transition state structure immediately before N_2 emission. In fact, the angular distribution of desorbing CO_2 in the CO oxidation on Pd(110) becomes broader at higher temperatures.[25] Therefore there must be a critical structure of the intermediate in the N_2O decomposition prior to N_2 emission.

The nascent N_2 is dominantly emitted nearly parallel to the surface plane without CO(*a*). Fractional amounts of the emitted N_2 at large desorption angles are suppressed in the presence of adsorbed CO in the range of the CO coverage between 1/4 and 1/2 ML. The dissociation yielding such large desorption angles may be prevented or the resultant N_2 is scattered by the nearest neighbor species located in the vicinity of the N_2 trajectory. In the absence of scattering by coadsorbed species, the collimation of desorbing N_2 is determined by a repulsive force along the ruptured N–O bond and the interaction between desorbing N_2 and the surface. The direction of N_2 desorption is controlled by a balance between the repulsive forces from surface rhodium atoms and those from the nascent oxygen atom. The axis of dissociated N_2O must be nearly parallel to the surface and oriented toward the [001] direction because the only possible repulsions acting parallel to the surface plane are those from the nascent oxygen along the ruptured N–O bond.

The energetics of such a highly excited N_2 has been previously proposed.[25] On Rh(110), the nascent oxygen may have high energy. For the process of $N_2O(a) \rightarrow N_2(g) + O(a)$, the energy that the product N_2 can carry away is given by $\Delta E_T = E_{N_2(g)} + E_{O(a)} - E_{N_2O(a,TS)}$, where $E_{N_2(g)}$, $E_{O(a)}$, and $E_{N_2O(a,TS)}$ are the potential energies of $N_2(g)$ and $O(a)$ and the transition state of $N_2O(a)$ dissociation, respectively. By assuming 400–500 kJ mol^{-1} as the bond energy of O–*M* (*M* stands for metal),[46] the available energy is estimated to be 240–340 kJ mol^{-1} because the dissociation of $N_2O(g) \rightarrow N_2(g) + O(g)(^3P)$ is endothermic by about 160 kJ mol^{-1} and the heat of adsorption of N_2O on Rh(110) is close to the activation energy of $N_2O(a)$ dissociation.[47,48] In this process, the emitted energy is dominantly released in the process of *M*–O bond formation.

On Rh(110), the nascent N_2 is emitted closely parallel to the surface plane with high kinetic energy. The mechanism of momentum transfer from the nascent oxygen atom to the outgoing N_2 is not clear at present. Probably, a sudden dilatation of the nascent oxygen atom acts to repel the N_2 molecule because some negative charge is likely to be transferred from the metal.[45] The operative repulsion between the nascent O(*a*) and N_2 has been examined by DFT, i.e., after the N_2O molecule is broken the wave-function symmetry is changed. The N_2 has an isolated N_2-like wave function, while the oxygen states hybridize with the metal states. At the region near the transition state, the N_2 and O are not yet far apart and the two wave functions overlap, resulting in Pauli repulsion between N_2 and O(*a*).[48]

The N_2 can receive high-energy impulse closely parallel to the surface plane. Such N_2 is likely to be scattered by coadsorbed species. On the other hand, the molecule that picks up less energy is emitted at a larger angle relative to the surface parallel because the repulsive force from the surface acting closer toward the surface normal becomes effectively stronger. This model is consistent with the results from the velocity analysis (i.e., the faster component emitted at large angles is suppressed at around 450 K) as well as with the results of the CO-PD work. The CO coverage decreases as the N_2O dissociation proceeds, i.e., the reaction takes place earlier at high CO coverage. The desorbed N_2 involves the desorption collimated at around 50°. The desorption collimated at around 70° is enhanced as the CO-PD proceeds. This collimation is also reproduced after the N_2 maximum, which is consistent with the results on Rh(110) covered by oxygen.[40] On clean Rh(110), the highly inclined N_2 desorption involves two components collimated at around 50° and 70°. This explains the high velocity and broad angular distributions on Rh(110). These two inclined desorption components with different kinetic energies and collimation angles are reminiscent of 193 nm photoinduced O_2 desorption on stepped surfaces.[49] Oxygen molecules on the surfaces align along the step edges. High-energy oxygen atoms (hot atoms) emitted by photons collide with the nearest and the next-nearest O_2 molecules, leading to inclined desorption with different collimation angles in the plane along the molecular axis.

On Pd(110), this CO effect was not observed because the N_2 desorption already collimates at around 45° without CO(*a*).[30]

D. Scattering by adsorbed CO

Adsorbed CO forms a $c(2\times2)$ lattice at 0.5 ML on Rh(110) and the CO–CO interaction in this lattice is

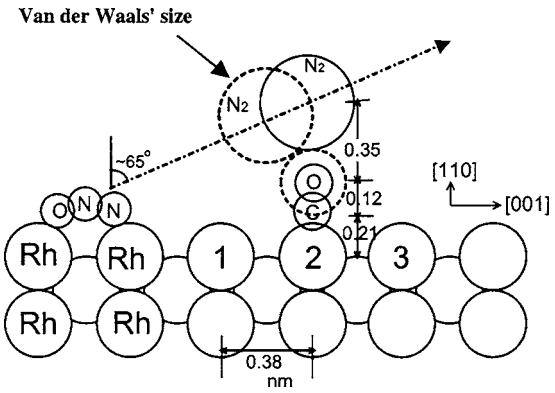

FIG. 9. A scattering model of the nascent N_2 by adsorbed CO on Rh(110). A side view of the configuration of N_2O, CO, and nascent N_2. The broken circles are drawn from the van der Waals radii. The inserted numbers stand for distances (in nm units).

repulsive.[39] This coverage is sufficiently high to prevent N_2O from dissociating. A side view of a possible N_2O+CO configuration is shown in Fig. 9. The broken circles denote the van der Waals radii of gaseous N_2 and the oxygen atom. Thus, roughly speaking, the outgoing trajectory of nascent N_2 will be unperturbed by scattering when the closest distance of outgoing N_2 to the oxygen atom in adsorbed CO exceeds the sum of the two van der Waals radii. The threshold angle below which the nascent N_2 can pass without being scattered is estimated to be about 65° off normal. The molecules leaving above this angle (closely parallel to the surface plane) will be scattered, i.e., the CO as close to N_2O as on site 2 (Fig. 9) would already scatter parts of the nascent N_2. The collimation angle should be smaller than this threshold value. In this estimation, the distance of the oxygen to the rhodium metal plane is 0.315 nm, referring to the analysis of CO on an atop site on Pt.[50,51] This angle shifts to 55° and 83° when CO occupies sites 1 and 3, respectively.

The scattering situation does not significantly change even when CO is located in a bridge position because CO is somewhat shifted upward and the sum of the van der Waals radii of N_2 and oxygen is large enough to cover the resultant scattering area for coverage above 1/4 ML.[50] The suppression of the large desorption angle component may also be due to the inhibition of the N_2O dissociation yielding such desorption. The scattering effect is supported by the enhanced cosine component at high CO pressures [Fig. 3(a)]. The product N_2 after scattering will desorb into the cosine form since the energy exchange between CO and N_2 is likely to be efficient because of the equal (close) mass.

In the present work, only CO(a), and not $N_2O(a)$ nor O(a), causes remarkable scattering. The amount of $N_2O(a)$ in the steady reduction is very small because of the small heat of adsorption and rapid decomposition above 400 K.[23] The amount of O(a) is also very small because of the reducing conditions.[30] Furthermore, the O finally adsorbs on fcc hollow sites in the trough, i.e., its height above the surface is minimal. On the other hand, CO stands on the surface, causing a steric barrier. It would be interesting to examine the collimation angle of desorbing N_2 in the N_2O+H_2 reaction. On Rh(110), the hydrogen desorption is completed at around 350 K.[52] The collimation angle under reducing conditions would remain unchanged in the temperature range of 400–550 K. The effect of H(a) itself would be interesting. This kind of experiment is now in progress.

E. Structure-informative desorption dynamics

In gaseous reactions, the chemical interaction field is commonly analyzed from the state-resolved spatial distributions of emitted products.[53] On the other hand, such analysis mostly becomes difficult on solid surfaces because nascent product molecules are likely to be trapped by dispersion or chemical adsorption forces and the energy transfer from the trapped product to the surface is very fast, in the order of picoseconds.[54] Only emitted products in limited exothermic desorption processes show hyperthermal energy and provide structural information.[9]

AR-product desorption analysis has opened a method to approach surface structures from reaction sides. It is in contrast to structural analysis from surface spectroscopies such as vibration spectroscopy, electron spectroscopy, and diffraction methods. The chemical reaction is completed in a very short period, in the order of femtoseconds, and the following energy relaxation is very fast. Thus, these methods are primarily based on the signal from nonreacting surface species, i.e., before the reaction or after the surface species has been thermalized and not during the event (i.e., not before thermalization). In AR desorption, on the other hand, surface-structural information is directly provided from the reaction event as the *crystal azimuth dependence* of the flux or translational and internal energies. This angle-resolved product desorption dynamics yields the orientation of intermediates directly emitting products as well as the symmetry and slope of product-formation sites.[9]

In this sense, measurements of the average energy of desorbing products over the surface or the reaction rates do not directly deliver structural information. A surface chemical reaction shows more or less its own structure sensitivity. The terminology "structure-sensitive reaction" was once used to classify reactions whose rates are extremely dependent on the surface structures, with a difference of a few orders of magnitude.[55] However, this classification does not provide information on the surface structures. Similarly, structural information is missing even when large differences are found in the energy of desorbing products among surfaces with different structures. Recently, while monitoring infrared emission, Kunimori and co-workers found remarkable differences in the vibrational temperatures of desorbing product CO_2 in the CO oxidation between Pd(111) and Pd(110) surfaces.[56–58] The internal energy would vary over the crystal azimuth if the light emission from the product is analyzed after AR procedures. The resultant anisotropy of the energy will be directly related to the site structure.

The main purpose of our AR measurements is to survey this anisotropy and not to examine the sharpness of the distribution as seen in ESDIAD.[59] In this sense, the internal energy of desorbing N_2 should be analyzed in both state-selective and AR ways in the next stage. This kind of work will provide detailed features of the surface reaction event. At present, the internal energy of desorbing products is fre-

quently analyzed in non-AR ways using resonance-enhanced multiphoton ionization[60,61] (REMPI) as well as infrared emission.

V. CONCLUSIONS

The angular distribution of desorbing product nitrogen has been examined in the N_2O decomposition in the range of 60–700 K. The results are summarized as follows. In the steady-state N_2O+CO reaction above 540 K, the N_2 desorption is sharply collimated at 64°–65° away from the surface normal and towards the [001] direction, whereas with decreasing surface temperature the collimation angle shifts towards the normal to 45° at 446 K. In the transient N_2O decomposition under CO pressure drop at 380–480 K, the N_2 desorption collimates at around 68° off normal. The N_2 desorption involves the components collimated at around 50° and 70°. In the transient N_2O decomposition on clean Rh(110) at 60–350 K, the product N_2 desorption collimates at 64°–68°. Adsorbed N_2O is oriented along the [001] direction prior to dissociation. The collimation angle shift is proposed to be due to the hindrance of N_2O dissociation or the scattering of nascent N_2 by CO molecules situated in the close vicinity of its outgoing trajectory.

ACKNOWLEDGMENTS

The authors thank Professor B. Gumhalter (Zagreb) and Dr. Y.-S. Ma for their critical discussion. The authors also thank Hiratsuka for analyzing data and drawing the figures. This work was partly supported by the Joint Studies Program (2005) of the Catalysis Research Center of Hokkaido University and Grant-in-Aid No. 18550114 for General Scientific Research from the Japan Society for the Promotion of Science. It was also supported in part by a 1996 COE special equipment program of the Ministry of Education, Science, Sports, and Culture of Japan.

[1] G. Centi, G. E. Arena, and S. Perathoner, J. Catal. **216**, 443 (2003).
[2] T. Matsushima, I. I. Rzeznicka, and Y.-S. Ma, Chem. Rec. **5**, 81 (2005).
[3] Y. Ohno, K. Kimura, M. Bi, and T. Matsushima, J. Chem. Phys. **110**, 8221 (1999).
[4] H. Horino, I. Rzeznicka, A. Kokalj, I. Kobal, Y. Ohno, A. Hiratsuka, and T. Matsushima, J. Vac. Sci. Technol. A **20**, 1592 (2002).
[5] R. H. Stulen, Prog. Surf. Sci. **32**, 1 (1989).
[6] R. D. Ramsier and J. T. Yates, Jr., Surf. Sci. Rep. **12**, 243 (1991).
[7] A. R. Burns, E. B. Stechel, and D. R. Jennison, Phys. Rev. Lett. **58**, 250 (1987).
[8] T. E. Madey, D. E. Ramaker, and R. Stockbauer, Annu. Rev. Phys. Chem. **35**, 215 (1984).
[9] T. Matsushima, Surf. Sci. Rep. **52**, 1 (2003).
[10] M. Kobayashi and Y. Tuzi, J. Vac. Sci. Technol. **16**, 685 (1979).
[11] G. Comsa and R. David, Surf. Sci. Rep. **5**, 145 (1985).
[12] H. H. Sawin and R. P. Merrill, J. Chem. Phys. **73**, 996 (1980).
[13] K. Watanabe, A. Kokalj, Y. Inokuchi, I. I. Rzeznicka, K. Ohshimo, N. Nishi, and T. Matsushima, Chem. Phys. Lett. **406**, 474 (2005).
[14] Y.-S. Ma, A. Kokalj, and T. Matsushima, Phys. Chem. Chem. Phys. **7**, 3716 (2005).
[15] A. Baraldi, S. Lizzit, D. Cocco, G. Comelli, G. Paolucci, R. Rosei, and M. Kiskinova, Surf. Sci. **385**, 376 (1997).
[16] N. R. Avery, Surf. Sci. **131**, 501 (1983).
[17] J. C. L. Cornish and N. R. Avery, Surf. Sci. **235**, 209 (1990).
[18] P. Väterlein, T. Krause, M. Bässler, R. Fink, E. Umbach, J. Taborski, V. Wüstenhagen, and W. Wurth, Phys. Rev. Lett. **76**, 4749 (1996).
[19] L. Schwaner, W. Mahmood, and J. M. White, Surf. Sci. **351**, 228 (1996).
[20] Y. Li and M. Bowker, Surf. Sci. **348**, 67 (1996).
[21] R. Sau and J. B. Hudson, J. Vac. Sci. Technol. **18**, 607 (1981).
[22] C. Kodama, H. Orita, and H. Nozoye, Appl. Surf. Sci. **121/122**, 579 (1997).
[23] K. Imamura, K. Imamura, H. Horino, I. Rzeznicka, A. Kokalj, I. Kobal, A. Hiratsuka, B. E. Nieuwenhuys, and T. Matsushima, Surf. Sci. **566–568**, 1076 (2004).
[24] R. A. Marbrow and R. M. Lambert, Surf. Sci. **67**, 489 (1977).
[25] I. I. Rzeznicka, Y.-S. Ma, G. Cao, and T. Matsushima, J. Phys. Chem. B **108**, 14232 (2004).
[26] G. Comelli, V. R. Dhanak, M. Kiskinova, N. Pangher, G. Paolucci, K. C. Prince, and R. Rosei, Surf. Sci. **260**, 7 (1992).
[27] G. Comelli, V. R. Dhanak, M. Kiskinova, K. C. Prince, and R. Roseil, Surf. Sci. Rep. **32**, 165 (1998).
[28] Y.-S. Ma, A. Kokalji, K. Shobatake, and T. Matsushima, J. Chem. Phys. **124**, 144711 (2006).
[29] I. I. Rzeznicka and T. Matsushima, Chem. Phys. Lett. **377**, 279 (2003).
[30] Y.-S. Ma, S. Han, and T. Matsushima, Langmuir **21**, 9529 (2005).
[31] T. Matsushima and Y. Ohno, Catal. Lett. **23**, 313 (1994).
[32] R. Imbihl, Prog. Surf. Sci. **44**, 185 (1993).
[33] S. W. Hla, P. Lacovig, G. Comelli, A. Baraldi, M. Kiskinova, and R. Rosei, Phys. Rev. B **60**, 7800 (1999).
[34] E. Schwarz, J. Lenz, H. Wohlgemuth, and K. Christmann, Vacuum **41**, 167 (1990).
[35] C. Africh, F. Esch, G. Comelli, and R. Rosei, J. Chem. Phys. **115**, 477 (2001).
[36] C. Africh, F. Esch, G. Comelli, and R. Rosei, J. Chem. Phys. **116**, 7200 (2002).
[37] V. R. Dhanak, G. Comelli, G. Cautero, G. Paulucci, K. C. Prince, M. Kiskinova, and R. Rosei, Chem. Phys. Lett. **188**, 237 (1992).
[38] A. Baraldi, V. R. Dhanak, G. Comelli, K. C. Prince, and R. Rosei, Surf. Sci. **293**, 246 (1993).
[39] J. J. Weimer, J. Loboda-Cackovic, and J. H. Block, Surf. Sci. **316**, 123 (1994).
[40] K. Imamura and T. Matsushima, Catal. Lett. **97**, 197 (2004).
[41] V. P. Zhdanov and T. Matsushima, Surf. Sci. **583**, 253 (2005).
[42] S.-W. Liu, H. Horino, A. Kokalj, I. Rzeznicka, K. Imamura, Y.-S. Ma, I. Kobal, Y. Ohno, A. Hiratsuka, and T. Matsushima, J. Phys. Chem. B **108**, 3828 (2004).
[43] K. Watanabe, A. Kokalj, H. Horino, I. Rzeznicka, K. Takahashi, N. Nishi, and T. Matsushima, Jpn. J. Appl. Phys., Part 1 **45**, 2290 (2006).
[44] A. Kokalj, I. Kobal, and T. Matsushima, J. Phys. Chem. B **107**, 2741 (2003).
[45] A. Kokalj and T. Matsushima, J. Chem. Phys. **122**, 034708 (2005).
[46] W. A. Brown, R. Kose, and D. A. King, Chem. Rev. (Washington, D.C.) **98**, 797 (1998).
[47] S. K. Ross, J. W. Sutherland, S.-C. Kuo, and R. B. Klemm, J. Phys. Chem. A **101**, 1104 (1997).
[48] I. Kobal, A. Kokalj, H. Horino, Y. Ohno, and T. Matsushima, Trends Chem. Phys. **10**, 139 (2002).
[49] S. Han, Y. Ma, and T. Matsushima, J. Chem. Phys. **123**, 094702 (2005).
[50] A. M. Lahee, J. P. Toennies, and Ch. Wöll, Surf. Sci. **177**, 371 (1986).
[51] J. D. Batteas, D. E. Gardin, M. A. Van Hove, and G. A. Somorjai, Surf. Sci. **297**, 11 (1993).
[52] W. Nichtl-Pecher, J. Gossmann, W. Stammler, G. Besold, L. Hammer, K. Heinz, and K. Müller, Surf. Sci. **249**, 61 (1991).
[53] D. Levine and R. B. Bernstein, *Molecular Reaction Dynamics* (Oxford University Press, New York, 1974), p. 181.
[54] E. J. Heiweil, M. P. Casassa, R. R. Cavanagh, and J. T. Stephensen, Annu. Rev. Phys. Chem. **40**, 143 (1989).
[55] M. Boudart, Adv. Catal. **20**, 153 (1969).
[56] H. Uetsuka, K. Watanabe, H. Kimpara, and K. Kunimori, Langmuir **15**, 5795 (1999).
[57] K. Nakao, S.-I. Ito, K. Tomishige, and K. Kunimori, J. Phys. Chem. B **109**, 17579 (2005).
[58] K. Nakao, S.-I. Ito, K. Tomishige, and K. Kunimori, Catal. Today **111**, 316 (2006).
[59] T. E. Madey and J. T. Yates, Jr., Surf. Sci. **63**, 203 (1977).
[60] H. A. Michelsen, C. T. Rettner, and D. J. Auerbach, in *Surface Reactions*, Springer Series in Surface Sciences Vol. 34, edited by R. J. Madix (Springer-Verlag, Berlin, 1994), p. 185.
[61] A. Hodgson, Prog. Surf. Sci. **63**, 1 (2000).